Kinetic Isotope Effects and Variable Reaction Coordinates in Barrierless Recombination Reactions

Craig A. Taatjes*

Combustion Research Facility, Mail Stop 9055, Sandia National Laboratories, Livermore, California 94551-0969

Stephen J. Klippenstein*,†

Department of Chemistry, Case Western Reserve University, Cleveland, Ohio 44106-7078

Received: April 30, 2001; In Final Form: July 2, 2001

The factors affecting kinetic isotope effects in barrierless recombination reactions are considered from the perspective of variational transition state theory (VTST). Despite the broad application of VTST methods, a general consideration of kinetic isotope effect predictions of the theory has not previously been undertaken, especially for cases where changes in the internal structure and vibrational frequencies of the fragments (i.e., the conserved modes) can be assumed to be negligible. Use of the center-of-mass separation as the reaction coordinate in such a case entails some restriction on the range of kinetic isotope effects which can be accommodated. Larger effects are possible within a variable reaction coordinate implementation of transition state theory, and the predicted kinetic isotope effects are shown to be strongly dependent on the location of the pivot point. Illustrative model calculations demonstrate the feasibility of reproducing the experimentally observed kinetic isotope effects for the CH + O_2, HCC + O_2, CH + C_2H_2, and CH + C_2H_4 reactions with realistic deviations of the pivot points from the center-of-mass. In contrast, calculations restricted to center-of-mass pivot points predict isotope effects that are even inverted. For the CH + CH_4 reaction, the isotope effects appear too large to be explained by the reaction coordinate variations, and changes in the conserved modes play a key role in the observed isotope effects, as demonstrated with ab initio based TST simulations. Overall, the experimentally observed kinetic isotope effects in CH addition reactions are strongly suggestive of an optimum reaction coordinate corresponding to a pivot point located near the center of the radical orbital.

I. Introduction

The measurement of kinetic isotope effects plays a key role in investigating details of chemical interactions.[1−3] Because the potential energy surface must remain the same for isotopic substitution, the change in atomic mass allows specific features of the interaction potential to be probed. The interpretation of kinetic isotope effects is generally based on transition state theory. In reactions proceeding through a well-defined barrier region, conventional transition state theory provides a physically compelling framework for both primary and secondary kinetic isotope effects. However, even for these reactions, variational minimization can have a significant impact on the kinetic isotope effect, especially where vibrational modes involving substituted atoms change frequency in the transition state region.[4,5]

In barrierless reactions, where the transition state must be determined variationally, there has been little investigation of kinetic isotope effects,[6−8] perhaps because they are expected to be close to the collision frequency ratio which is generally small. Indeed, for the H(D) + CH_3 reaction both center-of-mass reaction coordinate[6] and reaction path Hamiltonian based[8] variational transition state theory calculations predicted a kinetic isotope effect equal to the collision frequency ratio. However, recent experimental measurements show small but significant kinetic isotope effects for reactions of CH where no barrier exists to the reaction and where considerably exothermic product channels exist, ensuring negligible returning flux.[9−15] In this paper, we investigate the possible sources for kinetic isotope effects in such systems.

Applications of variational transition state theory (VTST) to barrierless recombination reactions commonly employ some form of a loose transition state approximation.[16−21] The central aspect of this approximation involves an assumed separation between the conserved modes, which correspond to vibrations of the separated molecules, and the remaining modes, termed the transitional modes. The transitional modes gradually transform their character throughout the transition state region as the rotations of the separated reactants couple together to form bending and torsional vibrations, and overall rotations in the adduct. The strict loose transition state approximation consists of neglecting changes in the conserved mode frequencies from their asymptotic values in the separated molecules, and, as a corollary, changes in their bond lengths and angles. The computational effort is therefore focused on the hindering potential and evaluation of the partition function for the transitional modes. In recent years, the introduction of variable reaction coordinate (VRC)−VTST,[22−29] where the reaction coordinate is chosen to be the distance between variationally optimized "pivot points" in the two reactant molecules, has significantly improved the calculation of rate coefficients for barrierless reactions.

* To whom correspondence should be addressed.
† Present address: Combustion Research Facility, Mail Stop 9055, Sandia National Laboratories, Livermore, CA 94551-0969.

10.1021/jp011632q CCC: $20.00
Published on Web 08/25/2001

The concentration on the transitional modes is understandable for computation of rate coefficients, which are determined by the total number of available states in the transition state region and hence depend most sensitively on the low frequency motions. The kinetic isotope effect, in contrast, arises from differences in numbers of states upon isotopic substitution and may be quite sensitive to variations in the conserved mode frequencies and zero-point energies along the reaction path. Furthermore, for a reaction coordinate specified by the separation between the centers-of-mass, the potential-independent component of the transitional mode contribution to the kinetic isotope effect reduces to the collision frequency ratio. The observation of kinetic isotope effects differing significantly from the collision frequency ratio would thus seem to provide data on changes in the frequencies of the conserved modes in the transition state, complementing the transitional-mode information available from rate coefficient measurements. However, as discussed below, more realistic reaction coordinates and transitional mode potentials may yield a significantly different transitional mode contribution to the kinetic isotope effect.

This article focuses on the role of a generalized reaction coordinate in explaining kinetic isotope effects in barrierless association reactions, such as those observed in the CH(CD) + O_2,[9] HCC(DCC) + O_2,[12] CH(CD) + C_2H_2,[13] CH(CD) + $C_2H_4(C_2D_4)$,[14] and CH(CD) + $CH_4(CD_4)$[13,15] reactions. As discussed in the experimental studies, each of these reactions is expected to be barrierless, and to have a highly exothermic saddlepoint for producing bimolecular products from the initially formed molecular complexes. The interested reader is referred to these works for more detail on the various product channels available and on the combustion significance of these reactions. Although specific comparisons with experiment are made here, the present analysis is qualitative and is aimed at a general investigation of the factors controlling kinetic isotope effects in VRC−VTST calculations, as is appropriate for the first detailed study of such effects. Thus, only simple model potential energy surfaces are employed in the analysis.

After discussing the importance of a variable reaction coordinate for transitional-mode contributions to the kinetic isotope effect, we also briefly consider the possible contribution to the kinetic isotope effect from variations in the conserved modes. For the CH + CH_4 reaction, some of the observed kinetic isotope effects are too large to be explained by the nature of the reaction coordinate, and so a somewhat more detailed analysis of the conserved mode variations is presented. However, we reiterate that the focus of this article is on the consideration of the possible magnitude of kinetic isotope effects that can be obtained from realistic pivot point deviations within the variable reaction coordinate transition state theory formalism. The goal is an overall framework for interpretation of kinetic isotope effects in barrierless reactions, not quantitative predictions for a few specific reactions.

To begin, a general loose transition state description for kinetic isotope effects is summarized in section II, with particular emphasis on the transitional mode contributions. Then, in section III, some illustrative model calculations of the transitional mode contribution are discussed. Included therein is a brief discussion of the features of the interaction potential that lead to optimization of the reaction coordinate away from the center of mass separation. Next, limited ab initio quantum chemical simulations provide the basis for estimates of the conserved mode contributions for CH reactions with acetylene, ethylene, and methane, as discussed in section IV. Finally, some concluding remarks are made in section V.

II. General Theory

A. VTST Description of Kinetic Isotope Effects. The interpretation of kinetic isotope effects begins with the transition state approximation, namely that the rate of reaction depends only on the characteristics of the reactive system near the critical transition state region. For a fixed transition state, this results in the familiar expression for the high-pressure limiting rate coefficient,

$$k_\infty(T) = g_e \frac{kT}{h} \frac{\sigma}{\sigma^\ddagger} \frac{Q^\ddagger(T)}{Q_{react}(T)} e^{-V^\ddagger/kT} \quad (1)$$

where Q_{react} is a partition function for the reactants, V is the potential energy along the reaction path, σ is the rotational symmetry number, and g_e is the electronic degeneracy factor. A double-dagger (‡) is used to denote quantities evaluated at the transition state. The pseudo-partition function for the transition state, $Q^\ddagger$, includes the $3N - 7$ vibrational modes orthogonal to the reaction coordinate.

The kinetic isotope effect for a fixed transition state is straightforwardly related to changes in vibrational frequencies between reactants and transition state. For a barrierless reaction, a quantitative description of the temperature dependence requires that the transition state be determined variationally. Here, as in most VTST analyses, we focus first on a canonical implementation, with a T-resolved minimization of the transition state partition function. Introducing a separation between the conserved modes (c) and the transitional modes (t), as in the loose transition state approximation, then yields

$$k_\infty(T) = g_e \frac{kT}{h} \frac{\sigma}{\sigma^\ddagger} \frac{Q_c^\ddagger(T)}{Q_c(T)} \frac{Q_t^\ddagger(T)}{Q_t(T)} e^{-V^\ddagger/kT} \quad (2)$$

A discussion of the assumptions involved in this separation of modes is provided in the Appendix for both this T-resolved case and also for the E-resolved case where the canonical transition state partition functions are obtained from minimizations of the microcanonical number of states. Notably, for the E-resolved case, the separation into a product of terms as in eq 2 requires an additional assumption of adiabatic conserved mode dynamics.

B. Center-of-Mass Reaction Coordinate. If the reaction coordinate is taken as the separation R of the centers of mass of the two reagent molecules, the description of the transitional mode partition function is greatly simplified. The transitional modes can then be expressed in terms of hindered rotations of the fragment molecules and overall rotation of the reacting system. Furthermore, the hindered rotor partition functions may be written in terms of free rotational partition functions and a configuration integral $\Phi(R,T)$ to yield[23,29,30]

$$k_\infty(T) = g_e \frac{kT}{h} \frac{\sigma}{\sigma^\ddagger} \frac{e^{-V^\ddagger/kT}}{Q_{trans}(T)} \left[\frac{Q_c^\ddagger(T)}{Q_{vib,1}(T) Q_{vib,2}(T)} \right] \left[\frac{Q_{pd}^\ddagger(T) Q_{fr,1}^\ddagger(T) Q_{fr,2}^\ddagger(T)}{Q_{fr,1}(T) Q_{fr,2}(T)} \right] \Phi^\ddagger(T) \quad (3)$$

where the double dagger now represents quantities calculated at the variationally determined transition state location. In this expression Q_{trans} denotes the canonical partition function for the relative translational motion of the two reactants, $Q_{vib,i}$ denotes that for the conserved vibrational modes of reactant i, Q_{pd} denotes the pseudo-diatomic partition function for the free orbital motion of the two fragments, and $Q_{fr,i}$ denotes the partition

function for free rotation of reactant i. The dependence on the transitional mode interaction potential is entirely contained in the factor $\Phi^{\ddagger}(T)$, which is the configuration integral, $\Phi(R,T)$, evaluated at the variationally determined value of the reaction coordinate, $R^{\ddagger}$[29]

$$\Phi(R,T) = \int e^{-V_t(\Omega;R)/kT} d\Omega / \int d\Omega \quad (4)$$

The transitional mode potential V_t is a function of the angular coordinates Ω describing the orientation of each of the fragments and of the line connecting them. It also depends parametrically on the reaction coordinate R.

The evaluation of the canonical VTST rate coefficient requires that a minimum in $k_\infty(T)$ is found by varying the reaction coordinate R. In principle, all of the transition state quantities can vary with R. The loose transition state assumption is often a very good approximation for barrierless association reactions, and provides an excellent starting point for consideration of the sources of kinetic isotope effects in such reactions. This approximation neglects changes in the geometries and force fields of the conserved modes, which means that any dependence of Q_c, $Q_{fr,1}$, and $Q_{fr,2}$ on R is neglected. Thus

$$Q_c^{\ddagger}(T) = Q_{vib,1}(T) Q_{vib,2}(T) \quad (5)$$

and

$$Q_{fr,1}^{\ddagger}(T) Q_{fr,2}^{\ddagger}(T) = Q_{fr,1}(T) Q_{fr,2}(T) \quad (6)$$

The part of the transitional mode partition function that corresponds to the orbital rotation of the complex has a simple dependence on R,

$$Q_{pd}^{\ddagger}(T) = \frac{8\pi^2 \mu kT}{h^2} R^2 \quad (7)$$

where the factor μ corresponds to the collision reduced mass for the two reacting fragments.

Thus, under the strict loose transition state assumption, and using the center-of-mass separation as the reaction coordinate, the VTST expression can be rewritten:

$$k_\infty(T) = g_e \frac{kT}{h} \frac{\sigma}{\sigma^{\ddagger}} \frac{e^{-V^{\ddagger}/kT}}{Q_{trans}(T)} Q_{pd}^{\ddagger}(T) \Phi^{\ddagger}(T) \quad (8)$$

Then, gathering together the factors that depend on the reaction coordinate yields

$$k_\infty(T) \propto \left(\frac{kT}{\mu}\right)^{1/2} \min[e^{-V(R)/kT} \Phi(R,T) R^2; R] \quad (9)$$

where the notation $\min[F(R);R]$ indicates minimization of the function $F(R)$ with respect to variation of R.

The predicted kinetic isotope effect, for any arbitrary interaction potential, can then be calculated as

$$\frac{k_H}{k_D} = \frac{(\mu_D)^{1/2} \min [e^{-V_H(R)/kT} \Phi(R,T) R^2; R]_H}{(\mu_H)^{1/2} \min [e^{-V_D(R)/kT} \Phi(R,T) R^2; R]_D} \quad (10)$$

where we have assumed that the ratio of symmetry numbers is unchanged by isotopic substitution. If the potentials V and V_t take the same value for the two isotopes at the same R and Ω, then the predicted isotope effect reduces analytically to the ratio of the collision frequencies, $(\mu_D/\mu_H)^{1/2}$. For symmetric substitutions in molecules with a center-of-symmetry (e.g., CH_4/CD_4, C_2H_4/C_2D_4, C_2H_2/C_2D_2) this isotopic independence of the potential is met and the predicted kinetic isotope effect properly reduces to $(\mu_D/\mu_H)^{1/2}$ for the center-of-mass reaction coordinate, regardless of the form of the interaction potential. We also note that in phase space theory [31−35] the potentials are explicitly assumed to be only R dependent, and the predicted isotope effect again reduces to the collision frequency ratio. However, in reality, the potential values for the same R and Ω generally do depend on the isotopic masses because the position of the center of mass is changed by isotopic substitution. Holding the center-of-mass separation fixed then leads to different atom−atom separations for different isotopic masses. Such effects are described in more detail below and are of course included in the model calculations presented in section III.

A similar result is obtained for the energy-resolved VTST treatment. As described in the Appendix, an assumption of vibrational adiabaticity for the conserved modes, together with the strict loose transition state assumption, allows for a separation of the transition state partition function into the product of the partition functions for the conserved and transitional modes. The expression for the rate coefficient then reduces to

$$k_\infty(T) = \frac{\int_0^\infty N^{\ddagger}(E) e^{-E/kT} dE}{hQ_{trans}(T)Q_c(T)Q_{rot}(T)} = \frac{Q_c^{\ddagger}(T) \int_0^\infty N_t^{\ddagger}(E) e^{-E/kT} dE}{hQ_{trans}(T)Q_c(T)Q_{rot}(T)} = \frac{\int_0^\infty N_t^{\ddagger}(E) e^{-E/kT} dE}{hQ_{trans}(T)Q_{rot}(T)} \quad (11)$$

The value for $N_t^{\ddagger}(E)$ is minimized for each energy, yielding an energy-dependent transition state location.

Thus, the problem of calculating the rate coefficient is again reduced to calculating the transitional mode partition function. The latter quantity can be written as a phase space integral, and the integral over the momenta can be carried out analytically, giving an expression for $N_t^{\ddagger}(E)$ which is reminiscent of eq 4[36−38]

$$N_t^{\ddagger}(E) \propto \int d\Omega \Phi(E,\Omega)|_{R=R^{\ddagger}} \quad (12)$$

with

$$\Phi(E,\Omega) \propto \frac{[E - V(\Omega)]^{n/2+1}}{B_0 \prod_{i=1}^{n} (B_i)^{1/2}} \quad (13)$$

where n is the total number of rotational degrees of freedom for the two reactants. The rotational constants of the separated fragments are denoted as B_i, and B_0 is the effective rotational constant for the orbital angular momentum,

$$B_0 = \frac{h^2}{8\pi^2 \mu R^2} \quad (14)$$

Placing eqs 12−14 into eq 11, collecting together the factors that depend on the reaction coordinate, and expressing the rotational and translational partition functions yields

$$k_\infty(T) \propto \frac{\int_0^\infty \min\{\int [E - V(\Omega)]^{n/2+1} R^2 d\Omega; R\} e^{-E/kT} dE}{\mu^{1/2} (kT)^{(n+3)/2}} \quad (15)$$

Because we are interested in the kinetic isotope effect, various

constant factors in the derivation of eq 15 have been suppressed. The ratio of the two isotopic reaction rate coefficients is now

$$\frac{k_H}{k_D} = \frac{\mu_D^{1/2}\int_0^\infty \min\{\int[E - V_H(\Omega)]^{n/2+1}R^2 d\Omega;R\}e^{-E/kT}dE}{\mu_H^{1/2}\int_0^\infty \min\{\int[E - V_D(\Omega)]^{n/2+1}R^2 d\Omega;R\}e^{-E/kT}dE} \quad (16)$$

Once again, for specific cases where the potential is isotopically invariant for a given R and Ω, this kinetic isotope effect can be analytically reduced to the collision frequency ratio. In most cases, however, the variation in the location of the center of mass will produce an isotope dependence of $V(R,\Omega)$ and contribute to the predicted kinetic isotope effect.

The most accurate VTST calculations optimize the transition state separately for each energy and total angular momentum J. The transition state sums of states then contain angular momentum terms which depend on the rotational constants for overall motion of the transition state (cf. eq 93 of ref 28), preventing the separation of mass-dependent terms used in the above discussion. A simple analytic reduction of the kinetic isotope effect appears infeasible for angular momentum conserving VTST, even with a strict loose transition state approximation and the center-of-mass separation reaction coordinate. Nonetheless, one does not expect major variations from the *E/J*-resolved to the *E*-resolved case above since the high pressure rates typically decrease by only about 10% upon inclusion of J resolution in the transition state determinations.

The VTST predictions for the kinetic isotope effect using a center-of-mass separation distance as the reaction coordinate can be simply summarized. Changes in the conserved mode frequencies can generate primary and secondary kinetic isotope effects according to the traditional TST expressions, and variational minimization can affect the degree to which these changing conserved mode frequencies are reflected in isotope dependence of the overall rate coefficient. In the absence of conserved mode frequency changes, use of a center-of-mass separation coordinate and an isotopically invariant potential (in center-of-mass frame coordinates) results in the collision frequency ratio for the calculated kinetic isotope effect. Deviations from the collision frequency ratio resulting from the isotopic dependence of the center-of-mass separation constrained potential are illustrated in section III.

The observation of kinetic isotope effects that exceed the collision frequency ratio, for example in the CH(CD) + O_2 and CH(CD) + hydrocarbon reactions, has been argued to imply conserved-mode frequency changes.[9,13] It would be convenient if an experimental measurement could be so unambiguously associated with conserved mode frequency changes. However, an improved definition of the dividing surface, provided by the implementation of variable reaction coordinate VTST, can be shown to provide significant kinetic isotope effects without changes in the conserved mode frequencies. This isotopic sensitivity is caused by the kinetic coupling of rotational motion to the redefined reaction coordinate. Exploring the effects of varying the reaction coordinate definition on the predicted kinetic isotope effect aids in the interpretation of experimental measurements and in determining when the involvement of conserved modes is implied.

C. Variable Reaction Coordinate. Calculations on many barrierless reactions have shown that a definition of the reaction coordinate that is allowed to deviate from the center-of-mass separation can result in a significant lowering of the calculated reaction rate coefficient, i.e., an improvement in the variational estimate of the transition state. The use of such a more general reaction coordinate s introduces the kinematic factor

$$\zeta = \frac{\mu\dot{s}}{p_R^*}\left|\frac{1}{\partial s/\partial R}\right| \quad (17)$$

into the variational optimizations. In this expression, $\dot{s}$ is the reaction coordinate velocity, and p_R^* is simply the value of $\mu\dot{R}$ which conserves energy. For the "variable reaction coordinate" scheme, where the reaction coordinates are implemented as distances between fixed points ("pivot points") in the molecular frame of the individual reactants, this factor can be written in terms of factors depending on partial derivatives of the reaction coordinate with respect to the rotational motions of the fragments[28]

$$\zeta = \left(\frac{\partial s}{\partial R}\right)^{-1}\left\{\left(\frac{\partial s}{\partial R}\right)^2 + \left[\left(\frac{\partial s}{\partial \vartheta_{0x}}\right)^2 + \left(\frac{\partial s}{\partial \vartheta_{0y}}\right)^2\right]\left(\frac{1}{R^2}\right) + \sum_{i=1}^{n}\frac{\mu}{I_i}\left(\frac{\partial s}{\partial \vartheta_i}\right)^2\right\}^{1/2} \quad (18)$$

The ϑ_i and I_i in eq 18 refer to rotational motions and moments of inertia of the fragment molecules, ϑ_{0x} and ϑ_{0y} to orbital motions of the complex. In the case where the fixed points coincide with the centers of mass, the center-of-mass separation coordinate is recovered and ζ reduces to unity.

For the *T*-resolved minimization of the transition state partition function, the average value over the spatial coordinates of

$$\left(\frac{\partial s}{\partial R}\right)^{-1}\left\{\left(\frac{\partial s}{\partial R}\right)^2 + \left[\left(\frac{\partial s}{\partial \vartheta_{0x}}\right)^2 + \left(\frac{\partial s}{\partial \vartheta_{0y}}\right)^2\right]\left(\frac{1}{R^2}\right) + \sum_{i=1}^{n}\frac{\mu}{I_i}\left(\frac{\partial s}{\partial \vartheta_i}\right)^2\right\}^{1/2} R^2 e^{-V(\Omega,R;s)/kT} \quad (19)$$

must be minimized as a function of the reaction coordinate s, while, for the *E*-resolved case, the average value over the spatial coordinates of

$$\left(\frac{\partial s}{\partial R}\right)^{-1}\left\{\left(\frac{\partial s}{\partial R}\right)^2 + \left[\left(\frac{\partial s}{\partial \vartheta_{0x}}\right)^2 + \left(\frac{\partial s}{\partial \vartheta_{0y}}\right)^2\right]\left(\frac{1}{R^2}\right) + \sum_{i=1}^{n}\frac{\mu}{I_i}\left(\frac{\partial s}{\partial \vartheta_i}\right)^2\right\}^{1/2} R^2[E - V(\Omega,R;s)]^{n/2+1} \quad (20)$$

is to be minimized. The generalized definition of the reaction coordinate then affects the predicted kinetic isotope effect through both the kinematic factor ζ (and the related R^2 term) and a potential energy dependent factor.

As discussed above for the center-of-mass separation coordinate R, the potential energy can depend on isotopic substitution through the isotopic variation in the atom−atom separations with orientation for a given reaction coordinate, thereby affecting the predicted kinetic isotope effect. However, for more chemical definitions of the reaction coordinate (e.g., bond separations) there is no isotopic variation of the potential for fixed s and Ω. Thus, for the chemical reaction coordinates there is no direct effect from the potential on the predicted isotope effects. The potential does still play a key role since the form and value of $s^\ddagger$ are largely determined by the details of the potential energy surface. In particular, from our experience, it is generally the angular dependence of the potential that determines the qualita-

tive shape of the transition state dividing surfaces, i.e., the location of the pivot points, and thus $s^{\ddagger}$. For example, the optimum dividing surfaces generally follow the attractive contours of the potential for modest angular displacements from the minimum energy path. Then, for larger displacements these dividing surfaces approach the repulsive regions of the potential as rapidly as is feasible, within the restricted functional forms employed for s.

The kinematic factor ζ, which is absent for the center-of-mass separation case, has a direct effect which depends on the rotational constants of the individual molecules, and hence on the isotopic substitution, even under the strict loose transition state assumption. It also has a secondary effect in slightly modulating the precise location of the pivot points. This secondary effect of ζ also leads to a minor further effect of the potential in that the optimum value of $s^{\ddagger}$ is now different for different isotopes and so different portions of the potential are sampled for different isotopes. In summary, for chemical definitions of the reaction coordinate, the details of the potential largely determine the location of the pivot points and thus the form and value of $s^{\ddagger}$, whereas the kinematic factor for the optimized $s^{\ddagger}$ largely determines the predicted kinetic isotope effect.

Immediately apparent from eq 18 is that the kinetic isotope effect arising from ζ requires coupling of the rotational motion of the fragments to the reaction coordinate s. The effect is larger for larger rotational constants (i.e., smaller moments of inertia I_i). The derivative couplings in eq 18 imply that any rotation of the fragment can contribute to ζ only if the pivot point is located away from the axis of rotation. For example, the change in the A rotational constant of a molecule upon isotopic substitution will contribute to the kinematic factor only if the pivot point for the fragment is located away from the A axis.

For the simple case of a linear rotor + atom reaction with the pivot point for the linear rotor taken to lie along its axis, the kinematic factor can be simply expressed as[29]

$$\zeta = \left[\frac{s^2 + (d\cos\theta + \sqrt{s^2 - d^2\sin^2\theta})^2\left(\frac{\mu d^2}{I_{\text{linear}}}\right)\sin^2\theta}{s^2 - d^2\sin^2\theta}\right]^{1/2} \qquad (21)$$

where d is the distance from the center-of-mass of the linear rotor to its pivot point, s is the distance from the pivot point to the atom, θ is the angle between the line of centers and the linear rotor axis (i.e., the Jacobi angle), and I_{linear} is the moment of inertia of the linear rotor. The form of the dependence of ζ_H and ζ_H/ζ_D on s, d, and θ is illustrated in Figure 1. For this illustration, $\mu_H = 8.88$ amu (the same as CH + C_2H_4) and $\mu_D = 9.33$ amu (the same as CD + C_2H_4), $I_{\text{linear},H}$ is set to 1.16 amu Å^2 (I_{CH}), and $I_{\text{linear},D}$ to 2.19 amu Å^2 (I_{CD}). This simple calculation gives a crude estimate of possible purely kinematic contributions to the kinetic isotope effect for CH(CD) reacting with C_2H_4.

The plots of the dependence of ζ_H and ζ_H/ζ_D on s and θ for a d value of 0.75 Å, provided in Figure 1a and 1b, indicate that the kinematic factor has only a modest variation with the value of the reaction coordinate s, which may be related to the near temperature independence of the observed kinetic isotope effects. The largest kinematic factors arise for angles near 90°, with, for this fairly typical d value (0.75 Å), the peak in the predicted kinetic isotope effect being about 1.3. However, the actual kinetic isotope effect would be substantially smaller because the angular values must be averaged over, with the largest contribution coming from angles where the potential is a

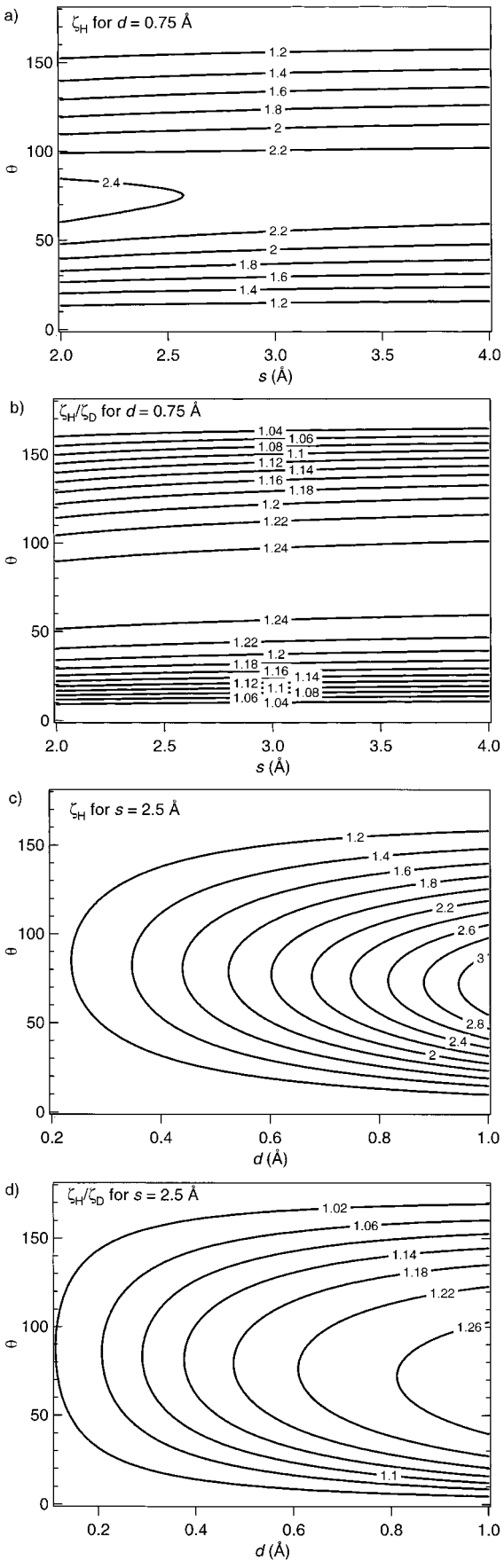

Figure 1. Dependence of the factor ζ in the case of an atom + diatom reaction on the Jacobi angular coordinate θ, the pivot point location d, and the reaction coordinate s. (a) Contour plot of ζ_H vs s and θ for d = 0.75 Å. (b) Same as (a) but a plot of ζ_H/ζ_D. (c) Contour plot of ζ_H vs d and θ for s = 2.5 Å. (d) Same as (c) but a plot of ζ_H/ζ_D.

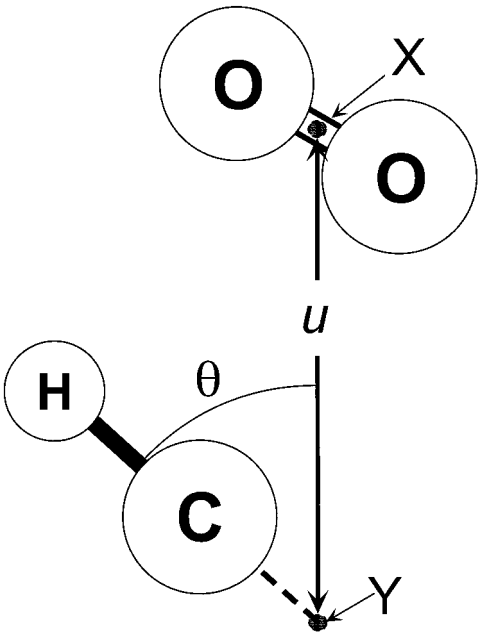

Figure 2. Schematic plot of the coordinates employed in the model potential, illustrated for $CH + O_2$.

minimum. Similar results are obtained for other d values as well, but with the magnitude of the effect gradually increasing with increasing d, as illustrated in Figure 1c and 1d, where the dependence of ζ_H and ζ_H/ζ_D on d and θ for a typical s value of 2.5 Å is plotted. In the absence of conserved-mode frequency changes, the ratio of the kinematic factors is expected to be the principal determinant of the kinetic isotope effect. These plots show that it is reasonable to expect, on a simple kinematic basis, CH/CD kinetic isotope effects between about 1.05 and 1.2.

III. Model Potential Calculations

A. Model Potential Forms. The accurate description of the potential energy surface in the transition state region for a barrierless reaction requires difficult and time-consuming ab initio simulations. The development of such potentials is far outside the scope of the present general study. Instead, this work focuses on the predicted isotope effects for realistic magnitude reaction coordinate variations in simple model potentials chosen to reproduce overall features of the experimentally investigated reactions. The aim of the present work is to investigate the sources of kinetic isotope effects in the VRC−VTST treatment, not to quantitatively analyze specific reactions.

To begin, a dummy atom, Y, is placed at a distance of 0.8 Å away from the radical C along the CH (or CCH) axis (cf. Figure 2). The use of this dummy atom simplifies the generation of a potential form that has the features observed in our prior studies of H + radical reactions, where the potential contours roughly follow the shapes of the radical orbital.[39−41] We write the potential as the product of radial and angular factors. The radial component of the model potential then involves a Varshni representation of the bonding interactions

$$V_{bond}(r) = D_e\left(1 - \frac{r_e}{r}\{1 - \exp[-\alpha(r_e^2 - r^2)]\}\right)^2 - D_e \quad (22)$$

where

$$r = u + 0.8(\text{Å}) \quad (23)$$

and u is the distance from the dummy atom Y to the center of the molecular fragment (labeled as dummy atom X here).

The angular dependence of the potential is represented as an exponentially modulated two point Fourier series

$$V_{bend}(\theta;u) = -f_0 \exp[-\gamma(u - u_e)]\left[\cos(\Delta\theta) - \frac{1}{4}\cos(2\Delta\theta) - \frac{3}{4}\right] \quad (24)$$

where θ is the XYC angle, $\Delta\theta$ is the deviation in θ from its equilibrium value θ_e, and f_0 and γ are two parameters which modulate the strength of the bending potential. For a given u, this angular form achieves its minimum value of 0 at $\Delta\theta = 0$, its maximum value of $2 f_0\exp[-\gamma(u-u_e)]$ at π, and has a period of 2π. Furthermore, the first and second derivatives at $\Delta\theta = 0$ are zero.

Thus, for small angular displacements from the minimum energy path the contours are parallel to spheres centered at the dummy atom Y, whereas for large displacements the potential becomes repulsive with a strength determined by f_0 and γ. Again, such an angular form qualitatively reproduces the observations from our studies of H + radical reactions. Another key aspect of this potential form is that it can yield an optimized fixed point for the radical that is displaced from the C atom, away from the center-of-mass, by about 0.8 Å.

In all cases, the interfragment torsional potentials are assumed to be negligible. Similarly, the potentials are assumed to be independent of the O_2 and C_2H_2 orientations. For the C_2H_4 fragment, mimicking the observed C_2D_4 isotope effects requires a similar description as for the radical component. Thus, the dummy atom X is displaced from the C_2H_4 center-of-mass by 0.8 Å along the symmetry axis perpendicular to the molecular plane. The r value is then redefined as u + 1.6 Å, and the bending potential is taken to be the sum of two components; one for each of the XYC and YXZ angles, where Z is now at the center-of-mass of the C_2H_4 molecule. This revised potential yields pivot points that are located near each of the two dummy atoms. The proper implementation of such pivot points requires the separate consideration of the contribution from each face of the C_2H_4 fragment.

For each of the potentials, we have set the equilibrium XYC bending angle θ_e equal to π. For the HCC reaction, this should be physically correct because the radical orbital is an sp hybrid orbital which lies along the HCC axis. For the CH reactions, the bonding in the transition state region is instead strongest at XYC angles closer to $\pi/2$. Thus, a physically correct potential for the CH reactions should use $\theta_e = \pi/2$, and would correspondingly yield optimum fixed points displaced off the linear axis. Unfortunately, the current VRC−VTST implementations are restricted to fixed points that lie along the linear axis due to the neglect of certain symmetry aspects. Thus, we have chosen here to simply explore the variation in the predicted isotope effects for potentials that produce displacements along the linear axis. The corresponding results will likely differ in quantitative detail from the physically correct ones, due to the different variations in the moments of inertia. However, they should still provide a qualitatively meaningful description of the size of isotope effect that can be obtained by varying pivot point locations.

The actual parameters employed for the various systems are summarized in Table 1. The choice of these parameters was based on various considerations. First, the optimized canonical VRC−VTST results should roughly reproduce the magnitude of the experimental observations. Second, the bonding potential should have a qualitatively realistic magnitude in the transition

TABLE 1: Model Potential Parameters

system	D_e (kcal/mol)	α (Å^{-2})	R_e (Å)	f_0 (kcal/mol)	γ (Å^{-1})
CH + O_2 (Pot 1)	85	0.38	1.2	380	1.5
CH + O_2 (Pot 2)	85	0.38	1.2	630	1.3
CH + O_2 (Pot 3)	85	0.38	1.2	1000	1.5
CCH + O_2	70	0.38	1.2	500	1.5
CH + C_2H_2	85	0.30	1.2	880	1.5
CH + C_2H_4	100.0	0.22	1.2	250, 500	1.5,1.5
CH + CH_4	85	0.50	1.2	940	1.5

state region. Also, the optimized pivot point locations should be reasonably close to the dummy atoms. Finally, the transition state location, and its variation with energy or temperature, should be similar to our observations for other systems. Note that although the values employed for f_0 appear large, they are not simply related to a bending force constant but instead describe the maximum repulsion for bending motions at fixed u value, which can of course be quite large. Furthermore, they have decayed significantly prior to the transition state region. The entry for the C_2H_4 case has two f_0 and γ values because there are two separate modes to be represented.

The model potentials described here provide a basis for isolating the role of the kinematic factor ζ in determining the kinetic isotope effect in barrierless reactions. Although the potentials are designed to reproduce qualitative features of the reactions under consideration, we reiterate that the aim of this investigation is to provide a general description of the various contributions to kinetic isotope effects in VRC−VTST calculations. The model potentials are clearly not intended to serve as an acceptable approximation for rate constant calculations. However, they enable modification of separate aspects of the potential energy surface and can provide physical insight into overall mechanism which is not readily available from more sophisticated and detailed calculations of individual reactions.

B. Results and Discussion. The variation of the calculated kinetic isotope effect with pivot point location was examined here via VRC−VTST calculations in which the separation R between the pivot points is optimized at the canonical level while the location of the pivot points is held fixed. A plot of this variation in the isotopic ratio $k_{CH + O_2}/k_{CD+O_2}$ as a function of d, the distance of the CH radical pivot point from its center-of-mass, is provided in Figure 3. The results plotted are for a temperature of 293 K, but they are essentially independent of temperature. For comparison the laser photolysis/chemiluminescence study of ref 9 observed kinetic isotope effects in the range from 1.16 to 1.21 (±∼0.08) for temperatures ranging from 293 to 720 K. The absence of any observed pressure dependence suggests that the observations should correspond to the high-pressure limit, as examined with the present calculations.

The experimental values roughly correspond to the calculations on the model potential for a pivot point that is 0.8 Å away from the center-of-mass. At the canonical level the optimized pivot points for the CH and CD reactions are displaced by 0.6 and 0.8 Å from the center-of-mass, respectively, yielding a kinetic isotope effect of 1.14. In contrast, for center-of-mass pivot points the kinetic isotope effect is calculated to be 0.975, whereas the collision frequency ratio is 1.026. Thus, for the CH + O_2 reaction, the consideration of realistic magnitude deviations in the pivot point locations can yield quantitative corrections to the predicted isotope effect.

Sample calculations indicate that the more appropriate energy E- and total angular momentum J-resolved optimizations yield only modest further reductions in the calculated kinetic isotope effects, and do not affect any of the qualitative conclusions. Thus, for simplicity, only T-resolved optimizations are considered here.

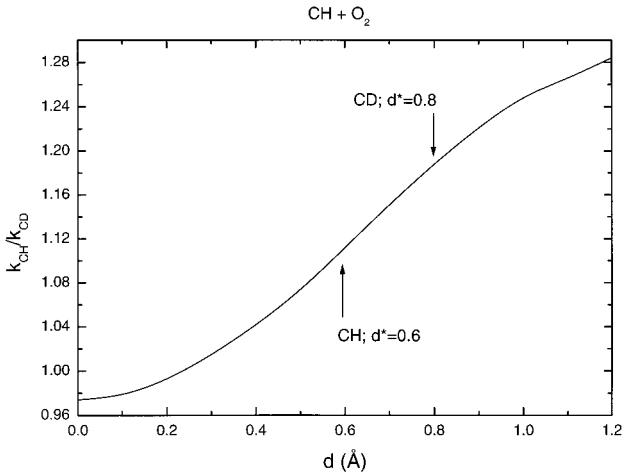

Figure 3. Plot of the kinetic isotope effect for the CH(D) + O_2 reaction as a function of the distance d from the radical pivot point to the CH(D) center-of-mass.

We have mentioned above that the variation of the location of the center of mass with isotopic substitution leads to a deviation from the collision frequency ratio for calculated kinetic isotope effects, even employing pivot points constrained to the centers-of-mass. The model potential calculations illustrate the magnitude of this deviation. For the present model potential the O_2 group bonds to the C side of the CH(CD) radical. Thus, for a given center-of-mass separation R, at the minimum energy orientation, the O_2 to C separation is smaller for CD as opposed to CH, and the potential is more attractive. Correspondingly, the optimized transition state separation R is larger in CD + O_2 than in CH + O_2. As a result, the factor in brackets in eq 10 is larger for D than for H, yielding a net reduction from the collision frequency prediction for the isotope effect. To confirm that the shift in center of mass location toward areas of more repulsive interaction is responsible for the deviation from the collision frequency ratio, we have also performed calculations for a "reversed" potential that corresponds to the O_2 group bonding to the H side of the CH radical. In this case, the above argument is inverted and one expects the calculated kinetic isotope effect to exceed the collision frequency ratio, as is indeed observed in the calculations.

The comparison in section II above of center-of-mass separation and variable reaction coordinate results suggests that the kinematic factor may dominate the kinetic isotope effect. Further calculations for two related potential forms substantiate that the VRC−VTST predictions for the isotope effects depend more strongly on the location of the optimized pivot points than on the details of the model potential form. For potential 2, the dummy atom X was moved to a separation of only 0.2 Å from the radical C atom, and the potential employed was otherwise analogous to the nominal potential form. For potential 3, the angular dependence of the nominal potential [cf. eq 21] was replaced with a sinusoidal hindered rotor. The optimized pivot point is at a separation of only 0.2 Å for both of these potentials, which would result in a calculated H/D isotope effect of only about 1.02 in both instances. However, as illustrated in Figure 4, the functional dependence on the pivot point location is remarkably similar to that for the nominal potential, indicating that the kinematic factor largely governs the kinetic isotope effect. This in turn suggests that the isotope effect is most sensitive to the location of the optimum pivot point (i.e., the

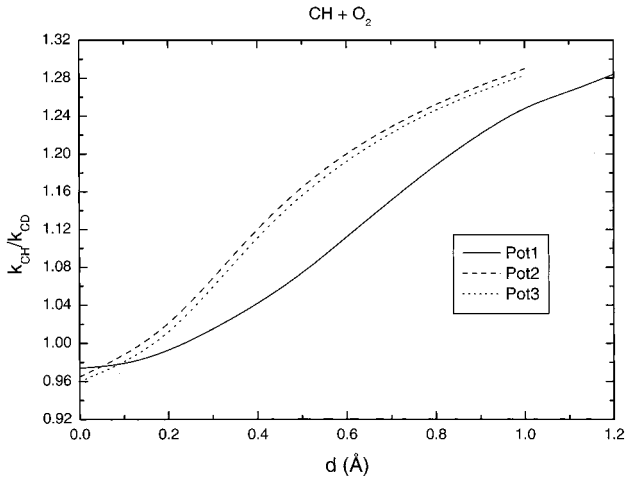

Figure 4. As in Figure 3, but also including results for model potentials 2 and 3.

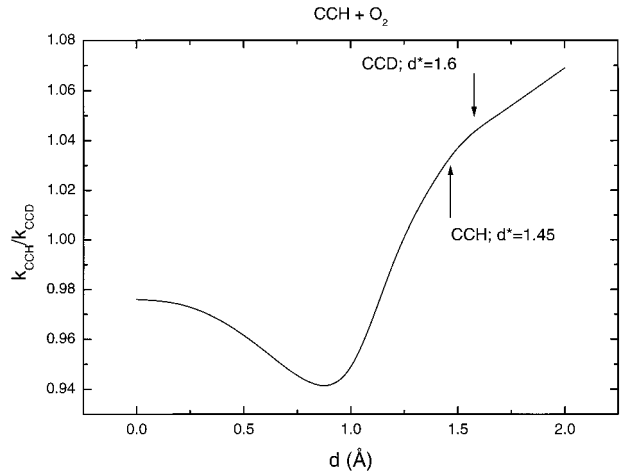

Figure 5. Plot of the CCH to CCD kinetic isotope effect for the CCH(D) + O_2 reaction as a function of the distance *d* from the CCH(D) pivot point to the CCH(D) center-of-mass.

nature of the reaction coordinate) and less sensitive to the details of the interaction potential.

The observed kinetic isotope effect for the HCC(DCC) + O_2 reaction is considerably smaller than that for the CH(CD) + O_2 reaction, being only 1.04 ± 0.03.[12] The kinetic isotope effect calculated from the model potential, as illustrated in Figure 5, is also substantially smaller, with the canonically optimized value being only 1.04. This reduction occurs even though the optimized pivot point for the HCC radical lies substantially further from its center-of-mass (d_{CCH} = 1.45 Å and d_{CCD} = 1.6 Å) than it does for the CH radical. The reduction in the magnitude of the variation in the isotope effects is related to the reduction in the variation of the rotational constants. The ratio of the CCH to CCD rotational constants is only 1.22, whereas that for CH to CD is 1.86. As a result, the kinematic factor ζ does not vary as much from one isotope to another for CCH.

For the remaining CH addition reactions, the variation in the CH/CD KIE with the value of *d* is qualitatively similar to that for the CH + O_2 reaction. A plot of the variation in the VRC−VTST calculation of the isotopic ratio $k_{CH + C_2H_2}/k_{CD+C_2H_2}$ as a function of *d*, the distance of the CH radical pivot point from its center-of-mass, is provided in Figure 6. For this reaction the KIE was observed to be 1.15 ± 0.03 at 291 K in the laser-photolysis/continuous-wave laser-induced fluorescence experimental study of ref 13, which corresponds to a *d* value of 0.7

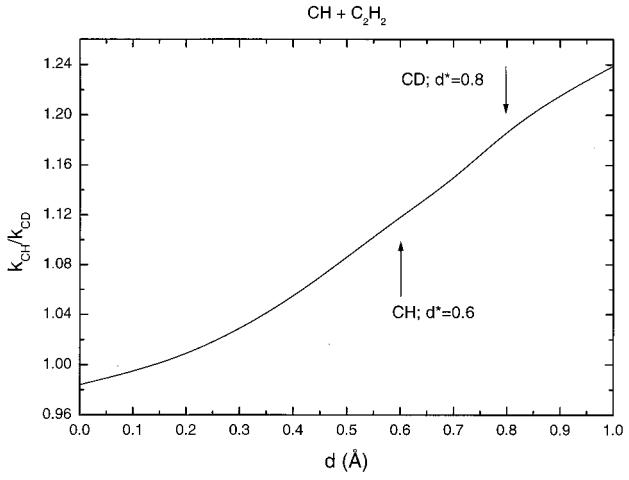

Figure 6. As in Figure 3, but for the CH(D) + C_2H_2 reaction.

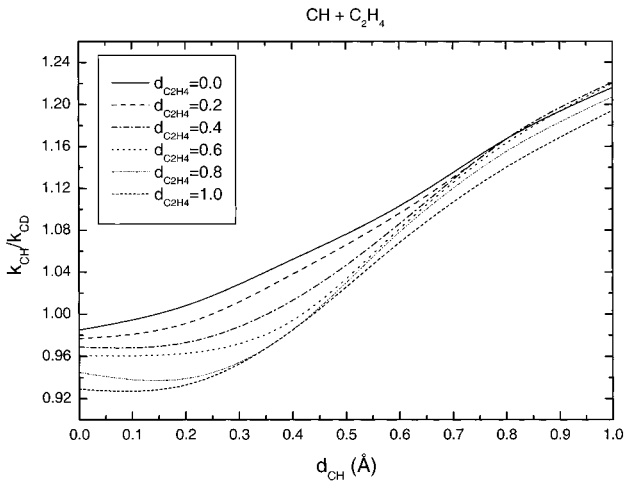

Figure 7. Plot of the CH to CD kinetic isotope effect for the CH(D) + C_2H_4(C_2D_4) reaction as a function of the distance *d* from the radical pivot point to the CH(D) center of mass.

Å. The canonical optimization of both *R* and *d* yields a kinetic isotope effect of 1.146. Both the calculated and observed kinetic isotope effects are essentially independent of temperature. Again, a realistic magnitude deviation of the pivot point location from the center-of-mass yields a quantitative correction for the kinetic isotope effect.

The C_2H_2 to C_2D_2 kinetic isotope effect was also measured for the CH + C_2H_2 reaction and it was found to be 1 within experimental uncertainty.[13] The cylindrical symmetry of the acetylene molecule makes it unlikely that its pivot point deviates substantially from the center-of-mass. Furthermore, because there is a center-of-symmetry in acetylene, the KIE for the center-of-mass case reduces to the collision frequency ratio of 1.01, in agreement with experiment.

The CH to CD and C_2H_4 to C_2D_4 kinetic isotope effects for the CH + C_2H_4 reaction were observed in laser photolysis/continuous wave laser-induced fluorescence experimental study to be 1.19 ± 0.04 and 1.08 ± 0.04, respectively, at 290 K.[14] The CH to CD KIE gradually decreases with increasing temperature reaching a value of 1.10 ± 0.02 at 720 K, while the C_2H_4 to C_2D_4 KIE is essentially constant. The VRC−VTST calculated dependence of the calculated CH to CD KIE on d_{CH} and $d_{C_2H_4}$ is illustrated in Figure 7. Locating the CH pivot point about 0.9 Å away from its center-of-mass again yields a prediction in agreement with experiment.

For the C_2H_4 to C_2D_4 KIE the center-of-mass coordinate again reduces to the collision frequency ratio of 1.02, due to the

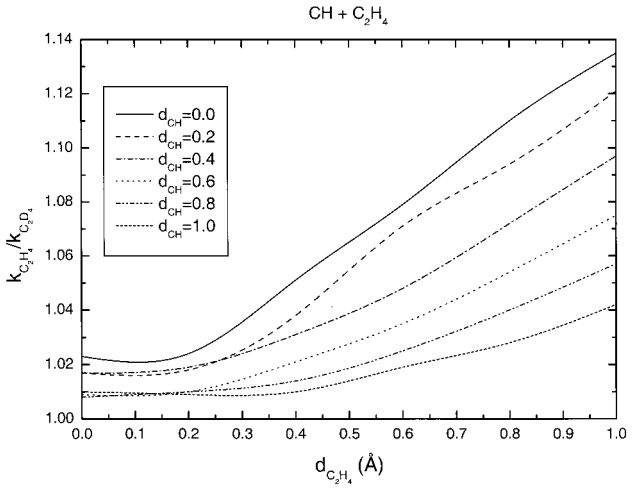

Figure 8. As in Figure 6, but for the C_2H_4 to C_2D_4 kinetic isotope effect as a function of the distance d from the $C_2H_4(C_2D_4)$ pivot point from its center of mass.

existence of a center-of-symmetry in C_2H_4. However, for C_2H_4 the pivot point is more likely to vary away from the center-of-mass (as compared to C_2H_2) due to the rotational asymmetry of the π-orbital binding space. Thus, the calculated dependence of the C_2H_4 to C_2D_4 KIE on the pivot point location is illustrated in Figure 8 for 290 K. The predicted KIE is seen to depend quite strongly on not just the C_2H_4 pivot point location, but also on that of the CH pivot point. Still, a deviation of about 1 Å again provides the right sort of magnitude for the KIE. The fact that model potential calculations provide qualitative agreement for the observed behavior of a range of reactions supports the interpretation that the kinematic factor dominates the kinetic isotope effect, and suggests that the kinetic isotope effect gives information on the nature of the reaction coordinate in the VTST framework.

The CH(CD) + $CH_4(CD_4)$ reaction is the final system for which we wish to consider kinetic isotope effects. For this system, the CH/CD and CH_4/CD_4 kinetic isotope effects were observed to be 1.23 ± 0.09 and 1.60 ± 0.13, respectively at 293 K.[13] Although not explicitly shown here, the CH/CD kinetic isotope effects can again be explained with reasonable magnitude deviations of the CH pivot point from its center-of-mass. In contrast, the CH_4/CD_4 KIE seems too large to explain simply with pivot point variations. The CH_4/CD_4 KIE for the center-of-mass reaction coordinate again analytically reduces to the collision frequency ratio, which is now 1.05. The somewhat large variation of a factor of 2 in all three of the rotational constants for CD_4 relative to CH_4 might at first be expected to yield an increased KIE relative to some of the other systems examined here. However, because methane is a spherical top, one axis of rotation can always be taken to contain the pivot point. Hence, only two of the CH_4 rotations contribute to the kinematic factor ζ, just as in the case of the CH molecule with the pivot point constrained to lie along the diatomic axis. The variation of the kinetic isotope effect with CH_4 pivot point displacement is therefore only slightly larger than that for the C_2H_4/C_2D_4 case, where the A rotational constant changes by a factor of 2 upon isotopic substitution, and should be similar to the variation seen for the CH radical (as shown in Figures 3 and 4). Clearly, the pivot point displacement required to match the experimental kinetic isotope effect in such a case would be physically unreasonable.

Moreover, the presence of four equivalent CH bonds to be attacked by the incoming CH suggests that there is little opportunity for improving the sampling of repulsive regions of the potential via optimizations of the pivot points, implying that the optimized CH_4 pivot point location should lie near the center of mass for chemically realistic potentials. The four equivalent CH bonds also make it somewhat more difficult to develop a practical potential and transition state model. For this reason, we have not explored this kinetic isotope effect with explicit VRC−VTST calculations and instead simply suggest that it is highly unlikely that pivot point variations within the variable reaction coordinate framework could yield an isotope effect of the magnitude observed experimentally.

IV. Ab Initio Potential Based Calculations. The model potential calculations described above provide an overall framework for considering the transitional mode contributions to kinetic isotope effects in barrierless addition reactions, and highlight the role of the kinematic factor which arises from the use of a generalized reaction coordinate. A comprehensive description of the kinetic isotope effects naturally requires consideration of possible variation in the conserved mode frequencies. For completeness, we therefore provide more detailed ab initio based calculations of several CH + hydrocarbon reactions which illustrate the role of conserved mode frequency variations.

A. Kinetic Isotope Effects in CH + CH_4. The reaction of CH with methane is somewhat different from the other reactions considered here in that there is no simple barrierless addition path. Instead, the formation of an adduct proceeds via insertion of the CH radical into one of the CH bonds to form an ethyl radical. The required rearrangements are likely to produce a significant saddle point on the potential energy surface. Furthermore, at this saddle point, the decoupling into conserved and transitional modes is likely to break down. Instead, the usual rigid-rotor harmonic-oscillator picture of the energetics is likely to be more meaningful.

The insertion path was examined at the MP4/6-311++G(*2d,p*)//MP2/6-31G* level in ref 42. These calculations suggest that there is indeed a saddle point, and that it is 0.2 kcal/mol below reactants. Later calculations at the MP2/6-311G** and MP2/6-311++G** levels failed to find a saddlepoint.[43] A reanalysis of the insertion saddlepoint is performed here with the goal of using the resulting vibrational and geometric information in a conventional transition state theory analysis. This reanalysis involves QCISD(T)/6-311++G** and MP2/6-311++G(3df,2pd) calculations carried out at geometries determined at the B3LYP/6-311++G** level. This procedure provides approximate QCISD(T)/6-311++G(3df,2pd) energies via the relation

$$\text{QCISD(T)/6-311++G(3df,2pd)} \cong \text{QCISD(T)/6-311++G**} + \text{MP2/6-311++G(3df,2pd)} - \text{MP2/6-311++G**} \quad (25)$$

With this approach the zero-point corrected saddle point energy is estimated to be −3.07 kcal/mol relative to reactants for the CH + CH_4 reaction. The average spin squared at the B3LYP and MP2 levels was 0.754 and 0.884, respectively. The zero-point corrected barriers for the CD + CH_4, CH + CD_4, and CD + CD_4 reactions differ by −0.6, +0.4, and −0.1 kcal/mol from that for the CH + CH_4 reaction. Subsequent CCSD(T)/6-31G** evaluations of the vibrational frequencies yield essentially identical zero-point energy corrections and closely analogous vibrational frequencies to those of the B3LYP calculations.

The rate constants and kinetic isotope effects evaluated for a rigid-rotor harmonic oscillator model employing the B3LYP/

TABLE 2: Rate Constants and Kinetic Isotope Effects for CH + CH_4

T (K)	k_{CH+CH_4}(expt)[a] 10^{-11}cm^3 s^{-1}	k_{CH+CH_4}(RRHO/TST) 10^{-11} cm^3 s^{-1}	CH + CH_4/ CD+CH_4[b]	CH + CD_4/ CD+CD_4[b]	CH + CH_4/ CH + CD_4[b]	CD+CH_4/ CD+CD_4[b]
200		1830	0.41	0.40	4.2	4.2
300	7.1 ± 0.3	112	0.60(1.22)	0.60(1.25)	2.8(1.57)	2.8(1.61)
450	5.0 ± 0.1	20.7	0.76(1.06)	0.76(1.03)	2.0(1.50)	2.0(1.46)
700	4.6 ± 0.1	8.49	0.87(1.07)	0.87(1.08)	1.59(1.48)	1.58(1.49)
1000		7.05	0.93	0.92	1.39	1.38
1400		8.12	0.96	0.95	1.28	1.28
2000		11.9	0.98	0.98	1.22	1.21

[a] Experimental measurements from ref 13 for a pressure of 100 Torr. [b] Calculated and experimental (ref 13, in parentheses) kinetic isotope effects.

6-311++G** structures and unadjusted vibrational frequencies and QCISD(T)/6-311++G(3df,2pd) energetics are summarized in Table 2. At low temperatures, the calculated rate constants are much greater than experiment due to the negative activation energy for the insertion saddle point. This discrepancy simply indicates that the dominant TS at low energies would be that for the initial approach to the weak complex preceding the saddle point. By 700 K, the theoretical estimate has nearly reached its minimum value, and is within a factor of 2 of the experimental rate constant, suggesting the dominance of the insertion saddle point by that temperature. The remaining overestimate is likely an indication of the need to variationally optimize the transition state for each energy and angular momentum contributing to the reaction.

Interestingly, at 700 K, where the RRHO transition state theory model is most meaningful, its prediction for the CH_4 to CD_4 kinetic isotope effect is in reasonable agreement with the experimental observation, suggesting that conserved-mode frequency variations are responsible for the kinetic isotope effect. However, the prediction for the CH to CD isotope effect is inverted. The latter discrepancy is likely an indication that one still needs to consider a more general reaction coordinate and the variational nature of the TS for the CH motion in order to properly predict this kinetic isotope effect.

B. Conserved Mode Variations in CH + C_2H_2 and CH + C_2H_4. For the CH + C_2H_2 reaction the vibrational frequencies were evaluated along the addition reaction path by Peeters and co-workers with B3LYP density functional theory.[44] These calculations indicate very modest variations in the conserved mode frequencies during the initial association. For example, the CH stretching frequency in the CH radical varies by 12 cm^{-1} or less from its infinite separation value for CC separations of 2.3 Å or greater. Furthermore, these variations are toward higher frequency, which would correspond to a CH to CD KIE of less than unity, in contradistinction with the experimental observations. The other conserved mode frequencies have a similar overall tendency to increase with decreasing separation and thus cannot be correlated with the observations. The CASSCF results of Walch,[45] which focus on an apparent saddle point at a CC separation of 2.5 Å, similarly suggest only modest variations, with that for the CH mode again increasing relative to separated reactants. Thus, one cannot explain the observed CH to CD KIE for the CH + C_2H_2 reaction with the calculated conserved-mode frequency variations.

For the CH + C_2H_4 reaction we have examined the force field along the addition reaction path at the CASSCF(7,7)/6-31G* level and at the B3LYP/6-31G** level. The 7 active orbitals in this CASSCF calculation consisted of the 5 valence orbitals of the CH radical plus the π and π^* orbitals of C_2H_4. There are again only modest variations in the CH stretching force constant until separations past (smaller CC values) that expected for the transition state. Furthermore, those modest variations again involve an increase rather than a decrease, and the variations in the remaining conserved modes are again too small and generally increasing. Thus, once again, it does not appear that variations in the conserved mode frequencies have any role in the observed kinetic isotope effects.

For both the CH + C_2H_4 and the CH + C_2H_2 reactions, the CH may also directly insert into one of the CH bonds in the molecule. For the CH + C_2H_4 reaction, we have determined the saddle point geometry and vibrational frequencies for the insertion at the B3LYP/6-31G** level. (Optimizations at the B3LYP/6-311+G** yield effectively no change in geometry and only a modest increase (~1 kcal/mol) in the energy.) At the ~QCISD(T)/6-311++G(3df,2pd) level (as for CH + CH_4) the saddle point was determined to lie 3.47 kcal/mol below reactants. The average spin squared for this saddle point was calculated to be 0.754 and 1.57 at the B3LYP and MP2 levels, respectively. The high spin contamination at the MP2 level suggests the need for some caution in interpreting the energetic predictions. However, we note that the QCISD(T) methodology is often capable of correcting for even such large spin contaminations.

Rigid-rotor harmonic oscillator calculations of the kinetic isotope effect for this path are similar to the above-described results for the CH + CH_4 insertion reaction, with a predicted C_2H_4/C_2D_4 kinetic isotope effect of about 1.3 to 1.4, and a predicted CH/CD kinetic isotope effect of about 0.95 to 1.0. However, comparison of the energetics and rates for the addition reaction path with those for the insertion path, suggests that the insertion reaction is unlikely to make a contribution of more than about 10%. Thus, the observed kinetic isotope effects for the CH + C_2H_4 reaction should largely correspond to that for the simple addition. A more detailed description of these findings has been provided previously.[14]

V. Concluding Remarks

Kinetic isotope effects for barrierless reactions have been explored using variational transition state theory with a variable reaction coordinate. Experimental investigations of CH reactions have shown small but significant kinetic isotope effects which cannot be explained by center-of-mass reaction coordinate calculations using a loose transition state assumption, that is to say, assuming no variation in the frequencies of conserved modes between reactants and transition state. The measured kinetic isotope effects had been construed to indicate a departure from the loose transition state picture.[9,13] The present work has shown that many of the observed kinetic isotope effects can be explained without conserved-mode frequency variations if more realistic reaction coordinates are employed in VTST calculations. In fact, with the exception of the large CH_4/CD_4 effect in the CH + methane reaction (which requires changes in conserved methane vibrations), the calculated kinetic isotope effects are

in relatively good agreement with experimental observations for pivot points corresponding roughly to the center of the radical orbitals involved in the incipient bond. It would be interesting to compare and contrast the predictions of the present variable reaction coordinate model with those of the reaction path Hamiltonian model, which has recently been revised to include approximate anharmonicity corrections.[46] The use of a variable reaction coordinate in transition state theory calculations not only provides an improved variational estimate of the rate coefficient, but appears to be essential for correctly describing the kinetic isotope effect in many systems.

Acknowledgment. This work is supported by the Division of Chemical Sciences, Geosciences, and Biosciences, the Office of Basic Energy Sciences, the U. S. Department of Energy

Appendix: Decoupling of the Conserved Modes in the Evaluation of Transition State Partition Functions

We review here the approximations necessary to obtain a decoupling of the conserved and transitional mode contributions to the canonical transition state partition function. When the variational minimization is performed at the canonical level, the transition state partition function may generally be written as

$$Q^{\ddagger}(T) = \frac{h^{1-n}}{k_B T}\min\left[\int dR d\mathbf{p}_R d\mathbf{q}_t d\mathbf{p}_t d\mathbf{q}_c d\mathbf{p}_c v_\perp \Theta(v_\perp)\delta(S) \exp(-\beta H);S\right] \quad \text{(A1)}$$

where $v_\perp$ is the velocity perpendicular to the dividing surface defined by S, and n is the number of degrees of freedom in the Hamiltonian H. The coordinates R, $\boldsymbol{q}_t$, and $\boldsymbol{q}_c$, denote a fragment−fragment radial separation, the fragment and orbital orientational coordinates, and the internal vibrational coordinates of the fragments, respectively. The momenta p_R, $\boldsymbol{p}_t$, and $\boldsymbol{p}_c$ are the corresponding conjugate momenta. The transitional modes can also be viewed as consisting of the overall rotational and relative bending and torsional motions of the two reacting fragments. The notation min[$F(S);S$] indicates minimization of the function $F(S)$ with respect to variation of S.

If the dividing surface S is independent of the conserved modes then the integral over $\boldsymbol{q}_c$ and p_c may be performed first to yield

$$Q^{\ddagger}(T) = \frac{h^{1-n_t}}{k_B T}\min\left[\int dR dp_R d\boldsymbol{q}_t d\boldsymbol{p}_t v_\perp \Theta(v_\perp)\delta(S) \exp(-\beta H_t) Q_c(T,R,p_R,\boldsymbol{q}_t,\boldsymbol{p}_t);S\right] \quad \text{(A2)}$$

where Q_c is the conserved mode canonical partition function for the given phase space point $(R,p_R,\boldsymbol{q}_t,\boldsymbol{p}_t)$ on the dividing surface S

$$Q_c(T,R,p_R,\boldsymbol{q}_t,\boldsymbol{p}_t) = \int d\boldsymbol{q}_c d\boldsymbol{p}_c \frac{1}{h^{n_c}} \exp[-\beta H_c(R,p_R,\boldsymbol{q}_t,\boldsymbol{p}_t)] \quad \text{(A3)}$$

The conserved mode Hamiltonian H_c is essentially that for the internal vibrations of the fragments (e.g., it would include the normal mode Hamiltonian for the conserved mode vibrations) but also builds in the coupling to the remaining degrees of freedom.

Assuming that this coupling [i.e., the dependence of H_c on $(R,p_R,\boldsymbol{q}_t,\boldsymbol{p}_t)$] may be written solely in terms of the dividing surface S, allows one to make the standard separation of the overall canonical partition function for the transition state in terms of the individual transitional and conserved mode canonical partition functions

$$Q^{\ddagger}(T) = \min\left[Q_t(T,S)Q_c(T,S);S\right] \quad \text{(A4)}$$

where

$$Q_t(T,S) = \frac{h^{1-n_t}}{k_B T}\int d\boldsymbol{q}_t d\boldsymbol{p}_t v_\perp \Theta(v_\perp)|\nabla S|\delta(S)\exp(-\beta H_t) \quad \text{(A5)}$$

and

$$Q_c(T,S) = \int d\boldsymbol{q}_c d\boldsymbol{p}_c \frac{1}{h^{n_c}} \exp[-\beta H_c(S)]. \quad \text{(A6)}$$

In standard applications the dividing surface S is represented in terms of a few scalar parameters, and the transition state partition function in eq A4 is minimized with respect to those scalar parameters. For example, for the center-of-mass reaction coordinate case the distance R, between the centers-of-mass of the two reacting fragments, specifies the dividing surface and the minimization with respect to S is replaced with a minimization with respect to R. For the variable reaction coordinate case, two additional vector parameters, $\boldsymbol{d_1}$ and $\boldsymbol{d_2}$, specifying the location of the pivot point for each fragment, are also used to define S and are treated as variables in the minimization process.

For a variational minimization at the E-resolved level, the canonical transition state partition function may be written as

$$Q^{\ddagger}(T) = \frac{1}{k_B T}\int_0^\infty dE \exp(-\beta E)\min\left[N(E,S);S\right], \quad \text{(A7)}$$

where the total number of states on the dividing surface S is given by

$$N(E,S) = \frac{h^{1-n}}{k_B T}\int d\boldsymbol{q} d\boldsymbol{p} v_\perp \Theta(v_\perp)\delta(S)\delta(E-H). \quad \text{(A8)}$$

A similar analysis to the above T-resolved analysis yields

$$Q^{\ddagger}(T) = \frac{1}{k_B T}\int_0^\infty dE \exp(-\beta E)\min\left[\int d\epsilon N_t(E-\epsilon,S)\rho_c(\epsilon,S);S\right], \quad \text{(A9)}$$

where $N_t(E,S)$ and $\rho_c(E,S)$ are the number and density of states for the transitional and conserved modes, respectively

$$N_t(E,S) = \frac{h^{1-n_t}}{k_B T}\int dR dp_R d\boldsymbol{q}_t d\boldsymbol{p}_t v_\perp \Theta(v_\perp)\delta(S)\delta(E-H_t) \quad \text{(A10)}$$

$$\rho_c(E,S) = \frac{1}{h^{n_c}}\int d\boldsymbol{q}_c d\boldsymbol{p}_c \delta[E-H_c(S)]. \quad \text{(A11)}$$

The convolution of the conserved and transitional modes prior to the minimization as in eq A9 corresponds to a statistical assumption for the distribution of energy among all the modes. This statistical assumption of transition state theory should be valid when there is a strong coupling of the conserved modes to the reaction coordinate or the transitional modes throughout the transition state region. With this statistical assumption the integration over ϵ properly ranges from 0 to E-$V_{min}(S)$, where $V_{min}(S)$ is the minimum potential value on the dividing surface S. The conserved and transitional modes are then inextricably coupled through the minimization process in eq A9. As a result,

even if the conserved mode geometries and force fields are strictly independent of S, one cannot write $Q^{\ddagger}(T)$ in terms of a separable product of conserved and transitional mode canonical partition functions. For this statistical assumption, the separability of the partition functions arises only when the minimization is replaced by the consideration of a single dividing surface S.

However, if, due to a weak coupling of the conserved modes to the remaining modes, the conserved mode vibrational dynamics are adiabatic, then the minimization and convolution should be interchanged yielding

$$Q^{\ddagger}(T) = \frac{1}{k_B T}\int_0^{\infty} dE \exp(-\beta E)\int_0^{E} d\epsilon \min\,[N_t(E-\epsilon,S)\rho_c(\epsilon,S);S] \quad \text{(A12)}$$

The upper limit for the ϵ integral is now reduced to E because any higher E's correlate with states that are asymptotically unavailable, i.e., for which $N_t(E-\epsilon,S)$ goes to zero at infinite separation. Now, if the conserved modes are independent of S, the conserved mode state density may be removed from the minimization to yield

$$Q^{\ddagger}(T) = \frac{1}{k_B T}\int_0^{\infty} dE \exp[-\beta(E-\epsilon)]\int_0^{E} d\epsilon \exp(-\beta\epsilon)\rho_c(\epsilon)\min\,[N_t(E-\epsilon,S);S] \quad \text{(A13)}$$

Reversing the order of integration then yields the desired mode separation

$$Q^{\ddagger}(T) = Q_c(T)Q_t^{\ddagger}(T), \quad \text{(A14)}$$

where

$$Q_c(T) = \int_0^{\infty} d\epsilon \exp(-\beta\epsilon)\rho_c(\epsilon), \quad \text{(A15)}$$

and

$$Q_t^{\ddagger}(T) = \frac{1}{k_B T}\int_0^{\infty} dE \exp(-\beta E)\min\,[N_t(E,S);S] \quad \text{(A16)}$$

Comparison of the theoretical predictions with experimental observations for the product state distributions in the unimolecular dissociation of species such as NCNO[39] and CH_2CO[40] suggests that adiabatic assumptions for the conserved mode motions are more meaningful than statistical assumptions, and correspondingly that the mode separability result is appropriate. In general, the adiabatic assumption for the conserved modes yields slightly lower partition functions than the statistical assumption. However, the differences are generally quite minor, typically being on the order of a few % or less.

References and Notes

(1) *Isotope Effects in Gas-Phase Chemistry*; Kaye, J. A., Ed.; American Chemical Society: Washington, D.C., 1992.

(2) Melander, L.; Saunders, W. H. Jr. *Reaction Rates of Isotopic Molecules*; John Wiley and Sons: New York, 1980.

(3) Truhlar, D. G.; Garrett, B. C.; Klippenstein, S. J. *J. Phys. Chem.* **1996**, *100*, 12771.

(4) Tucker, S. C.; Truhlar, D. G.; Garrett, B. C.; Isaacson, A. D. *J. Chem. Phys.* **1985**, *82*, 4101.

(5) Lu, D.-h.; Maurice, D.; Truhlar, D. G. *J. Am. Chem. Soc.* **1990**, *112*, 6206.

(6) Seakins, P. W.; Robertson, S. H.; Pilling, M. J.; Wardlaw, D. M.; Nesbitt, F. L.; Thorn, R. P.; Payne, W. A.; Stief, L. J. *J. Phys. Chem. A* **1997**, *101*, 9974.

(7) Harding, L. B.; Troe, J.; Ushakov, V. G. *Phys. Chem. Chem. Phys.* **2000**, *2*, 631.

(8) Hase, W. L.; Mondro, S. L.; Duchovic, R. J.; Hirst, D. M. *J. Am. Chem. Soc.* **1987**, *109*, 2916.

(9) Taatjes, C. A. *J. Phys. Chem.* **1996**, *100*, 17840.

(10) Taatjes, C. A. *J. Chem. Phys.* **1997**, *106*, 1786.

(11) Taatjes, C. A. *J. Chem. Phys.* **1997**, *107*, 10829.

(12) Thiesemann, H.; Taatjes, C. A. *Chem. Phys. Lett.* **1997**, *270*, 580.

(13) Thiesemann, H.; MacNamara, J.; Taatjes, C. A. *J. Phys. Chem. A* **1997**, *101*, 1881.

(14) Thiesemann, H.; Clifford, E. P.; Taatjes, C. A.; Klippenstein, S. J. *J. Phys. Chem. A* **2001**, *105*, 5393.

(15) Blitz, M. A.; Johnson, D. G.; Pesa, M.; Pilling, M. J.; Robertson, S. H.; Seakins, P. W. *J. Chem. Soc., Faraday Trans.* **1997**, *93*, 1473.

(16) Gilbert, R. G.; Smith, S. C. *Theory of Unimolecular and Recombination Reactions*; Blackwell Scientific Publications: Oxford, 1990.

(17) Baer, T.; Hase, W. L. *Unimolecular Reaction Dynamics*; Oxford University Press: Oxford, 1996.

(18) Chesnavich, W. J.; Bowers, M. T. *Prog. Reaction Kinetics* **1982**, *11*, 137.

(19) Wardlaw, D. M.; Marcus, R. A. *Adv. Chem. Phys.* **1987**, *70*, 231.

(20) Hase, W. L.; Wardlaw, D. M. In *Bimolecular Collisions*; Ashfold, M. N. R., Baggott, J. E., Eds.; Royal Society of Chemistry: London, 1989.

(21) Klippenstein, S. J. In *The Chemical Dynamics and Kinetics of Small Radicals*; Liu, K., Wagner, A. F., Eds.; World Scientific: Singapore, 1995; Vol. 1.

(22) Klippenstein, S. J. *Chem. Phys. Lett.* **1990**, *170*, 71.

(23) Klippenstein, S. J. *J. Chem. Phys.* **1991**, *94*, 6469.

(24) Klippenstein, S. J. *J. Chem. Phys.* **1992**, *96*, 367.

(25) Klippenstein, S. J. *Chem. Phys. Lett.* **1993**, *214*, 418.

(26) Klippenstein, S. J. *J. Phys. Chem.* **1994**, *98*, 11459.

(27) Smith, S. C. *J. Phys. Chem.* **1994**, *98*, 6496.

(28) Smith, S. C. *J. Chem. Phys.* **1999**, *111*, 1830.

(29) Robertson, S. H.; Wagner, A. F.; Wardlaw, D. M. *Faraday Discuss.* **1995**, *102*, 65.

(30) Robertson, S. H.; Wagner, A. F.; Wardlaw, D. M. *J. Chem. Phys.* **1995**, *103*, 2917.

(31) Klots, C. E. *J. Phys. Chem.* **1971**, *75*, 1526.

(32) Pechukas, P.; Rankin, R.; Light, J. C. *J. Chem. Phys* **1966**, *44*, 794.

(33) Pechukas, P.; Light, J. C. *J. Chem. Phys.* **1965**, *42*, 3281.

(34) Nikitin, E. E. *Teor. Eksp. Khim. Acad. Nauk. Ukr. SSR* **1965**, *1*, 135.

(35) Nikitin, E. E. *Teor. Eksp. Khim. Acad. Nauk. Ukr. SSR* **1965**, *1*, 428.

(36) Smith, S. C. *J. Phys. Chem.* **1993**, *97*, 7034.

(37) Smith, S. C. *J. Chem. Phys.* **1991**, *95*, 3404.

(38) Smith, S. C. *J. Chem. Phys.* **1992**, *97*, 2406.

(39) Klippenstein, S. J.; Harding, L. B. *Phys. Chem. Chem. Phys.* **1999**, *1*, 989.

(40) Klippenstein, S. J.; Harding, L. B. *Proc. Combust. Inst.* **2000**, *28*, 1503.

(41) Harding, L. B.; Klippenstein, S. J. *Proc. Combust. Inst.* **1998**, *27*, 151.

(42) Wang, Z.-X.; Huang, M.-B.; Liu, R.-Z. *Can. J. Chem.* **1997**, *75*, 996.

(43) Wang, Z. X.; Huang, M. B. *J. Chem. Soc., Faraday Trans.* **1998**, *94*, 635.

(44) Vereecken, L.; Pierloot, K.; Peeters, J. *J. Chem. Phys.* **1998**, *108*, 1068.

(45) Walch, S. P. *J. Chem. Phys.* **1995**, *103*, 7064.

(46) Song, K.; Hase, W. L. *J. Phys. Chem. A* **2001**, *105*, 2453.